

Optical ISAC: Fundamental Performance Limits and Transceiver Design

Alireza Ghazavi Khorasgani[✉], Mahtab Mirmohseni[✉], Ahmed Elzanaty[✉]
5/6GIC, Institute for Communication Systems (ICS), University of Surrey, Guildford, United Kingdom
{a.ghazavi, m.mirmohseni, a.elzanaty}@surrey.ac.uk

Abstract—This paper characterizes the optimal capacity-distortion (C-D) tradeoff in an optical point-to-point (P2P) system with single-input single-output for communication and single-input multiple-output for sensing (SISO-SIMO-C/S) within an integrated sensing and communication (ISAC) framework. We introduce practical, asymptotically optimal maximum a posteriori (MAP) and maximum likelihood estimators (MLE) for target distance, addressing nonlinear measurement-to-state relationships and non-conjugate priors. Our results show these estimators converge to the Bayesian Cramér-Rao bound (BCRB) as sensing antennas increase. We also demonstrate that the achievable rate-CRB (AR-CRB) serves as an outer bound (OB) for the optimal C-D region. To optimize input distribution across the Pareto boundary of the C-D region, we propose two algorithms: an iterative Blahut-Arimoto algorithm (BAA)-type method and a memory-efficient closed-form (CF) approach, including a CF optimal distribution for high optical signal-to-noise ratio (O-SNR) conditions. Additionally, we extend and modify the Deterministic-Random Tradeoff (DRT) to this optical ISAC context.

Index Terms—Optical Integrated Sensing and Communication (O-ISAC), Bayesian Cramér-Rao Bound (BCRB), optimal input distribution, modified Deterministic-Random Tradeoff (DRT)

I. INTRODUCTION

Future wireless networks aim to integrate advanced sensing with communication, essential for applications like intelligent transportation and smart cities. Integrated sensing and communication (ISAC) systems epitomize this convergence, sharing hardware, spectrum, and signaling for both sensing and communication (S&C) [1]. While radio frequency (RF) ISAC has been the primary focus, optical ISAC (O-ISAC) is emerging as a promising complement, particularly in free space optics (FSO) systems, which offer unique advantages in optical communication and sensing [2].

Previous work [3] explored the optimal capacity-distortion (C-D) and outage tradeoff for single-antenna RF ISAC systems. The optimal estimator simplifies to the linear minimum mean-square error (LMMSE) estimator under specific conditions (e.g., Gaussian priors), but real-world scenarios often involve nonlinear functions of sensing response channel (SRC) and non-conjugate priors, such as estimating distance from an echo signal, which complicates the computation of the optimal estimator [4]. Significant research has addressed the achievable rate-Cramér-Rao bound (CRB) (AR-CRB) tradeoff in single-input single-output for communication and single-input multiple output for sensing (SISO-SIMO-C/S) RF channels, particularly for parameters like angle of departure (AoD) and angle of arrival (AoA) [5]–[8]. However, gaps remain in practical estima-

tors, transceiver design, and optimal C-D regions. Additionally, most studies have focused on Gaussian signaling, which may not fully exploit the potential benefits for ISAC. To enhance observations, one solution is to record multiple feedbacks across several channel uses with block-wise independent, identically distributed (i.i.d.) states (block length T). While this improves sensing performance, it degrades communication performance proportionally to T^{-1} , especially for large T [5, Eq. 36]. To the best of our knowledge, O-ISAC systems have not been explored in terms of information-theoretical fundamental limits.

This paper characterizes the optimal Pareto boundary of achievable rate-distortion (AR-D) and C-D regions for an optical point-to-point (P2P) SISO-SIMO-C/S ISAC system, using multiple antennas to improve both communication and sensing, particularly for target distance estimation with nonlinear SRC relationships and non-conjugate priors. We extend and modify the deterministic-random tradeoff (DRT) [5] to optical SISO-SIMO-C/S ISAC and general estimators, introducing practical, asymptotically optimal estimators. We analyze the performance of our proposed maximum a posteriori (MAP) and maximum likelihood estimator (MLE) estimators, demonstrating their convergence to the CRB as the number of sensing antennas increases. Additionally, we show that in asymptotic scenarios, AR-CRB can serve as an outer bound (OB) for MAP, MLE, and any unbiased estimator within optimal C-D region. We propose two algorithms to determine the optimal input distribution for the Pareto boundary of the C-D region, validate these algorithms against the endpoints, and characterize the optimal O-ISAC input distribution under high optical signal-to-noise ratio (O-SNR) conditions.

Notation: Sets are denoted by calligraphic letters (e.g., \mathcal{X}), with cardinality $|\mathcal{X}|$. Real numbers are \mathbb{R} ; nonnegative reals are \mathbb{R}_0^+ . Random variables are uppercase (e.g., X), and realizations are lowercase (e.g., x). Vectors are boldfaced (e.g., \mathbf{Y}_s). Key symbols include \sim (distribution), $\perp\!\!\!\perp$ (independence), and $\stackrel{d}{\sim}$ (asymptotic distribution). Functions/operators: $\mathcal{N}(\mu, \sigma^2)$ (Gaussian), $\mathcal{H}(\cdot)$ (entropy), $\mathcal{I}(\cdot)$ (mutual information (MI)), $\mathbb{E}_X[\cdot]$ (expectation), $|\cdot|$ (absolute value), and $\|\cdot\|$ (norm).

II. SYSTEM MODEL

We consider a P2P O-ISAC system (see Fig. 1) with a single-antenna transmitter (Tx), an n_s -antenna monostatic sensing receiver (Sens. Rx) (collocated with Tx), a single-antenna communication receiver (Comm. Rx), and a point-wise target. This setup, typical for Light Detection and Ranging (LiDAR)

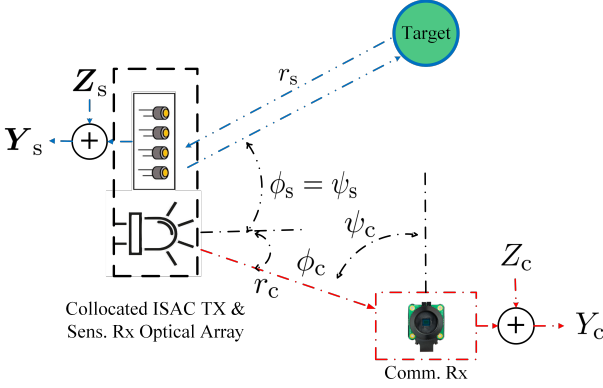


Fig. 1: O-ISAC system with memoryless channels.

evaluations [9], transmits data to Comm. Rx while estimating the target distance $R_s \in \mathbb{R}_0^+$, with realization r_s , based on echoes at Sens. Rx. We employ a state-dependent FSO ISAC channel with intensity modulation / direct detection (IM/DD) detected by both receivers [10], [11].

Communication and Sensing Models: The received signal at Comm. Rx during the i -th channel use is:

$$Y_{c,i} = h_c X_i + Z_{c,i}, \quad (1)$$

where $h_c \in \mathbb{R}$ is the line-of-sight (LoS) communication channel (CC), X_i is the transmitted signal, and $Z_{c,i} \sim \mathcal{N}(0, \sigma_c^2)$ is i.i.d. additive white Gaussian noise (AWGN). The CC is:

$$h_c = \frac{A}{r_c^2} R_0(\phi_c) T_s(\psi_c) g(\psi_c) \cos \psi_c \cdot \mathbf{1}_{[0, \text{FOV}]}(\psi_c), \quad (2)$$

where r_c is the distance between Tx and Comm. Rx, ϕ_c and ψ_c are angles relative to Tx and Comm. Rx, $T_s(\cdot)$ is the concentrator gain, A is the effective area, and FOV is the field of view (FOV). The Tx radiant intensity gain is $R_0(\phi) = \frac{(m+1)}{2\pi} \cos^m \phi$, where $m = -\frac{\ln 2}{\ln(\cos \Phi_{1/2})}$ [10].

The echo signal received at Sens. Rx at the i -th channel use is:

$$\mathbf{Y}_{s,i} = \mathbf{h}_s(R_{s,i}) X_i + \mathbf{Z}_{s,i}, \quad (3)$$

where $\mathbf{h}_s(R_{s,i}) \in \mathbb{R}^{n_s \times 1}$ is the target response coefficient dependent on $R_{s,i}$, and $\mathbf{Z}_{s,i} \sim \mathcal{N}(0, \sigma_s^2 \mathbf{I}_{n_s})$. The target response matrix $\mathbf{h}_{s,j,i}(r_{s,j,i})$ is:

$$h_{s,j,i}(r_{s,j,i}) = \frac{\text{RCS}}{r_{s,j,i}^4} R_0(0) T_s(\psi_s) g(\psi_s) \cos \psi_s \cdot \mathbf{1}_{[0, \text{FOV}]}(\phi_s), \quad (4)$$

where $\text{RCS} = A^2 R_0(\phi_s) T_s(0) g(0) R_0(0) T_s(\psi_s) g(\psi_s) \cos \phi_s$ is the radar cross section (RCS), assuming perfect RCS and no additional noise from reflection [12]. With Sens. Rx antennas in a uniform linear array (ULA) and the target moving along a straight line, ψ_s and ψ_c remain constant¹. Assuming $r_s \gg \Delta r_s$, we have $r_{s,j,i} \approx r_{s,i}$ for all i, j ².

Code Definition: A $(2^{nR}, n)$ code for state-dependent memoryless channel with delayed feedback (SDMC-DF) includes:

¹Phase shifts are immeasurable in IM/DD [10].

²A uniform 8×8 array with $11.2 \mu\text{m}$ spacing ensures a FOV of 8° [13].

(1) a discrete message set \mathcal{M} with $|\mathcal{M}| = 2^{nR}$, (2) encoding functions $\phi_i : \mathcal{M} \times \mathcal{Y}_s^{i-1} \mapsto \mathcal{X}$ for $i = 1, 2, \dots, n$, (3) a decoding function $f : \mathcal{R}_s^n \times \mathcal{Y}_c^n \mapsto \mathcal{M}$, and (4) a state estimator $h : \mathcal{X} \times \mathcal{Y}_s^n \mapsto \hat{\mathcal{R}}_s^n$, with $\hat{\mathcal{R}}_s$ as the reconstruction alphabet. For a given code, the random message M is uniformly distributed over \mathcal{M} , and inputs are generated as $X_i = \varphi_i(W, \mathbf{Y}_s^{i-1})$ for $i = 1, \dots, n$. The channel outputs $Y_{c,i}$ and $\mathbf{Y}_{s,i}$ at time i depend on state $R_{s,i}$ and input X_i via the transition laws $P_{Y_c|X, R_s}(\cdot | x_i, r_{s,i})$ and $P_{Y_s|X, R_s}(\cdot | x_i, r_{s,i})$, given in (3) and (1). Let $\hat{\mathcal{R}}_s := (\hat{R}_{ss,1}, \dots, \hat{R}_{ss,n}) = h(X^n, \mathbf{Y}_c^n)$ denote state estimate at Tx, and $\hat{W} = g(\mathcal{R}_s^n, \mathbf{Y}_c^n)$ the decoded message at Comm. Rx³. The quality of state estimation is measured by the expected average per-block distortion: $\Delta^{(n)} := \mathbb{E}[d(\mathcal{R}_s^n, \hat{\mathcal{R}}_s^n)] = \frac{1}{n} \sum_{i=1}^n \mathbb{E}[d(R_{s,i}, \hat{R}_{ss,i})]$, where $d : \mathcal{R}_s \times \hat{\mathcal{R}}_s \rightarrow \mathbb{R}_0^+$ is a bounded distortion function with $\max_{(r_s, \hat{\xi}) \in \mathcal{R}_s \times \hat{\mathcal{R}}_s} d(r_s, \hat{\xi}) < \infty$. In practical optical systems, X is proportional to optical intensity and thus nonnegative: $X \in \mathbb{R}_0^+$. Then, $\mathbb{E}[|X^n|] = \frac{1}{n} \sum_{i=1}^n \mathbb{E}[|X_i|]$.

Definition 1. (C-D Region) A C-D tuple (C, D) is achievable with power budget P if there exists a sequence of $(2^{nR}, n)$ codes that satisfies:

$$\Delta^{(n)} \leq D, \quad \mathbb{E}[|X^n|] \leq P, \quad P_e^{(n)} \rightarrow 0. \quad (5)$$

Here, $P_e^{(n)} \triangleq \frac{1}{2^{nR}} \sum_{i=1}^{2^{nR}} \mathbb{P}\{\hat{M} \neq i | M = i\}$ and $d(r_s, \hat{\xi}) = (r_s - \hat{\xi})^2$ is the squared error distortion. C-D region $C_P(D)$ for power budget P is defined as $C_P(D) = \sup\{R | (R, D) \text{ is achievable with } P\}$.

In the next section, we characterize C-D region for O-ISAC system. We first describe optimal estimator h , which, independent of encoding and decoding functions, operates on a single input symbol with n_s -fold feedback. Specifically, it estimates $\hat{R}_{ss,i}$ based solely on X_i and $\{\mathbf{Y}_{s,j,i}\}_{j=1}^{n_s}$, without considering other feedback signals $\{\mathbf{Y}_{s,j,i'}\}_{i' \neq i}$.

Lemma 1. The deterministic minimum mean-square error (MMSE) estimator $\hat{\xi}$, which minimizes the expected distortion, depends on x and $\mathbf{y}_s := \text{vec}\{\mathbf{y}_{s,j}\}_{j=1}^{n_s}$ and is given by

$$\hat{\xi} = \mathbb{E}_{R_s}[R_s | X = x, \mathbf{Y}_s = \mathbf{y}_s]. \quad (6)$$

The distortion $\Delta^{(n)}$ is minimized by the estimator, regardless of the encoding and decoding functions:

$$h^*(x^n, \mathbf{y}_s^n) := (\hat{\xi}^*(x_1, \mathbf{y}_{s,1}), \dots, \hat{r}_s^*(x_n, \mathbf{y}_{s,n})). \quad (7)$$

The estimation cost for each input symbol $x \in \mathcal{X}$ is

$$c(x) = \int P_{R_s} \int P_{\mathbf{Y}_s|X, R_s} \times (r_s - \hat{\xi}(x, \mathbf{y}_s))^2 d\mathbf{y}_s dr_s. \quad (8)$$

Proof. Refer to Appendix A. \square

Lemma 1 shows that optimal estimator depends only on the current feedback observations $\mathbf{Y}_{s,i}$ due to the memoryless SRC. Thus, the sensing cost is a function of the input signal, $c(x)$ [3, Lemma 1].

³The monostatic Sens. Rx, collocated with Tx, knows X^n [5]. It estimates R_s from \mathbf{Y}_s^n , while Comm. Rx decodes M from \mathbf{Y}_c^n .

III. MAIN RESULT

In this section, we characterize AR-D region using: (i) A Blahut–Arimoto Algorithm (BAA)-type algorithm for general signal-independent (S-I) noise channels, (ii) A closed-form (CF) solution for high O-SNR (for Comm. Rx) scenarios, (iii) A time sharing (TS)-based scheme between communication optimal (Comm. Opt.) and sensing optimal (Sens. Opt.) modes. In addition, we propose AR-D regions, based on performing: (i) The MAP estimator (Section III-A), (ii) The MLE (Section III-B), (iii) Bayesian CRB (BCRB)-based yielding OB(Section III-C). To determine C-D region for the joint distribution $P_X P_{R_s} P_{Y_c|X R_s} P_{Y_c|X R_s} P_{R_s|X, y_s}$, we use the result of [3] by setting the channel state to R_s .

$$\underset{P_X}{\text{maximize}} \quad \mathcal{I}(X; Y_c | R_s), \quad (9a)$$

$$\text{subject to} \quad \int_{x \in \mathcal{X}} x P_X(x) \leq P, \quad (9b)$$

$$\int_{x \in \mathcal{X}} c(x) P_X(x) \leq D, \quad (9c)$$

$$\int_{x \in \mathcal{X}} P_X(x) = 1. \quad (9d)$$

1) TS-Based Scheme This scheme, is based on time-sharing between the following two modes:

1-1) Comm. Opt.: Ignoring the distortion constraint, (9) reduces to finding the channel capacity $\mathcal{C}(h_c, P)$ of an optical channel with coefficient h_c and average power constraint P . The exact capacity is unknown but is bounded by its upper bound (UB) [14, Theorem 8] and lower bound (LB) [15, Example 12.2.5].

$$\mathcal{C}_{\text{LB}}(h_c, P) = \frac{\frac{1}{2} \ln(h_c P) - \sqrt{\frac{\pi \sigma^2}{2h_c P}} + \frac{1}{2} \ln(1 + \frac{2}{h_c P})}{\ln 2} + \frac{\sqrt{h_c P(2 + h_c P)} - h_c P - 1}{\ln 2}, \quad (10)$$

$$\mathcal{C}_{\text{UB}}(h_c, P) = \frac{1 - \ln(\frac{1}{P}) + \ln(h_c)}{\ln 2} + o_P(1). \quad (11)$$

Here, $o_P(1)$ approaches zero as $P \rightarrow \infty$.

1-2) Sens. Opt.: In this mode, (9) simplifies to finding the input distribution that minimizes average sensing distortion, formulated as:

$$\underset{P_X}{\text{maximize}} \quad \int_{x \in \mathcal{X}} c(x) P_X(x), \quad (12a)$$

$$\text{subject to} \quad (9b), (9d). \quad (12b)$$

Lemma 2. The optimal solution to (12) is $P_X^{\text{Sens. Opt.}}(x) = \delta(x - x^*)$, where $x^* := \arg \min_{x \leq P} c(x)$. This distribution yields zero MI and the minimum distortion $D_{\min} = c(x^*)$.

Proof. Refer to Appendix C. \square

2) Optimal AR-D Region: BAA for General, CF for High O-SNR Regime: In the high O-SNR regime (O-SNR :=

$\frac{\mathbb{E}[X]}{\sigma_c^2} \gg 1$), where $\mathcal{H}(Y_s | X)$ is independent of P_X , (9) simplifies due to additive noise⁴.

$$\underset{P_X}{\text{maximize}} \quad \mathcal{H}(X | R_s) \stackrel{(a)}{=} \mathcal{H}(X), \quad (13a)$$

$$\text{subject to} \quad (9b), (9c), (9d) \quad (13b)$$

where (a) follows from $X \perp\!\!\!\perp R_s$ as per [3, Theorem 1]. Since (13) is a convex problem with concave entropy $\mathcal{H}(X)$ and affine constraints, it can be solved using the Karush–Kuhn–Tucker (KKT) method [16].

Lemma 3. The solution to (13) is given by

$$p_X(x) = \exp(1 - \eta_1 - \eta_2 x - \eta_3 c(x)), \quad (14)$$

Here, η_1 is the normalization constant, while $\eta_2 \geq 0$ and $\eta_3 \geq 0$ are the dual variables for the power budget and sensing constraint, respectively.

Proof. The result follows from entropy definitions and the Lagrangian derivative. Details are omitted for brevity. \square

To solve (9) and derive optimal C-D region, we use the BAA method [17, Section VI] for the general case and lemma 3 for the high-O-SNR regime. We introduce two non-negative penalty factors, η_2 and η_3 . For each fixed η_3 (representing a given distortion level), the optimal η_2 is determined by complementary slackness. Specifically, if $\eta_2 = 0$ satisfies the power budget constraint, then $\eta_2^* = 0$; otherwise, $\eta_2^* > 0$, and we adjust η_2 using gradient descent (GD) [16] to satisfy the power budget constraint with equality. The detailed algorithm is provided in Appendix B.

Remark 1. In Comm. Opt. mode, we can set η_3 in (14) to zero, which results in an exponential distribution. This confirms the result presented in [14].

To compute (6), we need $P_{R_s|X, y_s}(r_s | x, y_s)$:

$$P_{R_s|X, y_s}(r_s | x, y_s) = \frac{P_{y_s|X, R_s} P_{R_s}}{\int_{r_s \in \mathcal{R}_s} P_{y_s|X, R_s} P_{R_s}}. \quad (15)$$

However, computing (15) is generally intractable due to the complexity of the marginal distribution [4].

Lemma 4. Let $\hat{r}_{s\text{MAP}}$ and $\hat{r}_{s\text{MP}}$ denote MAP estimate $\arg \max_{r_s \geq 0} P_{R_s|X, y_s}(r_s | x, y_s)$ and the mean posterior (MP) estimate $\mathbb{E}_{r_s}[P_{R_s|X, y_s}(r_s | x, y_s)]$, respectively. Then, as $n_s \rightarrow \infty$, $\hat{r}_{s\text{MAP}} \rightarrow \hat{r}_{s\text{MP}}$ in probability and $P_{R_s|y_s, X}$ has a Gaussian probability density function (PDF). Specifically, $\hat{\xi} \stackrel{a}{\sim} \mathcal{N}(r_s, I^{-1}(r_s))$.

Proof. By the Bernstein–von Mises theorem [18] and [19, Theorem 11.3], for a large sample size n_s , $P_{R_s|X, y_s}(r_s | x, y_s)$ is asymptotically normal with mean $\hat{r}_{s\text{MP}}$ and variance Σ_n , where Σ_n is the inverse of the Fisher information (FI) matrix. Therefore, MAP estimate $\hat{r}_{s\text{MAP}}$, which is the mode of the (15), converges to the mean of the (15) $\hat{r}_{s\text{MP}}$. \square

⁴:

A. MAP-Based Achievable ISAC C-D Region

Theorem 1. MAP estimator $(\arg \max_{r_s \geq 0} P_{R_s|X, \mathbf{y}_s}(r_s | x, \mathbf{y}_s))$ is $\hat{\xi} \in \mathcal{R}_s$ that satisfies:

$$\frac{\lambda \sigma_s^2}{n_s} \hat{\xi}^9 + 4RCSx \left(\frac{1}{n_s} \sum_{j=1}^{n_s} y_{s,j} \right) \hat{\xi}^4 - 4RCS^2 x^2 = 0, \quad \hat{\xi} \geq 0. \quad (16)$$

Proof. Setting the curvature of the logarithm of (15) with respect to (w.r.t.) r_s to zero. \square

Eq. (16) can be solved numerically for any $x \in \mathcal{X}$ and $\mathbf{y}_s \in \mathcal{Y}_s$ using methods such as Newton-Raphson. Deriving an analytical PDF for MAP estimate is generally infeasible [19]. Instead, we use computer simulations for performance assessment, as detailed in Section IV.

B. MLE-Based Achievable ISAC C-D Region

Lemma 5. Define MLE as

$$\hat{r}_{s,MLE} = \arg \max_{r_s \geq 0} P_{\mathbf{y}_s|X, R_s}(\mathbf{y}_s | x, r_s)$$

As $n_s \rightarrow \infty$, MAP estimate approaches MLE.

Proof. As $n_s \rightarrow \infty$, the logarithm of 15 is dominated by the sum term $\sum_{s=1}^{n_s} (\mathbf{y}_s - \frac{RCSx}{r_s^4})^2$, while the term $-\lambda r_s$ becomes negligible in comparison. Thus, the logarithm of 15 approximates the $\log(P_{\mathbf{y}_s|X, R_s}(\mathbf{y}_s | x, r_s))$ function, which corresponds to MLE. Hence, MAP estimate converges to MLE as $n_s \rightarrow \infty$. \square

Lemma 6. Let $u : \mathbb{R}^{n_s \times 1} \times \mathbb{R} \rightarrow \mathbb{R}$ be a one-to-one function. MLE of $R_s(\mathbf{h}_s, x) := u(\mathbf{h}_s x) = \sqrt[4]{\frac{xRCS}{h_s}}$, where the PDF $P_{\mathbf{Y}_s|\mathbf{h}_s, X}$ is parameterized by \mathbf{h}_s (given X). MLE of R_s is:

$$\hat{R}_s = u(x\hat{H}_s),$$

where \hat{H}_s is MLE of \mathbf{h}_s , obtained by maximizing $P_{\mathbf{Y}_s|\mathbf{h}_s, X}$.

Proof. Refer to [19, Theorem 7.2]. \square

Theorem 2. MLE for estimating h_s is simply the mean of the observations: $\hat{h}_s = \frac{1}{x} \frac{1}{n_s} \sum_{j=1}^{n_s} \mathbf{Y}_{s,j}$. Thus MLE for estimating

$$r_s \text{ is, } \hat{\xi} = \begin{cases} \sqrt[4]{\frac{RCSx}{\frac{1}{n_s} \sum_{j=1}^{n_s} \mathbf{Y}_{s,j}}} & \text{if } \frac{RCSx}{\frac{1}{n_s} \sum_{j=1}^{n_s} \mathbf{Y}_{s,j}} \geq 0, \\ \text{MLE is not valid} & \text{otherwise.} \end{cases}$$

Proof. $\hat{h}_s = \frac{1}{x} \min_{h_s \in \mathbb{R}^+} \|\mathbf{y}_s - \mathbf{h}_s(R_s)\mathbf{1}_{n_s}\|^2$ is an least squares (LS) problem with a CF solution [16]. \square

C. BCRB-Based Approach: OB

Theorem 3. BCRB for any unbiased estimator \hat{R}_s of R_s , with realization r_s , is given by: $BCRB(x | r_s) = \frac{1}{\frac{16n_s RCS^2 x^2}{\sigma_s^2} r_s^{-8} + \lambda}$.

Proof. Refer to Appendix D. \square

Lemma 7. The BCRB($r_s | x$) is asymptotically convex in r_s as either n_s or O-SNR (or both) increase.

Proof. Refer to Appendix E. \square

Remark 2. The BCRB is a valid lower bound for the mean-square error (MSE) of an estimator \hat{R}_s^* only if the estimator is unbiased [19, Theorem 3.1]. A sufficiently large n_s ensures this condition. Additionally, for large datasets, MLE is known to be asymptotically unbiased and achieves BCRB [19, Theorem 11.3].

Lemma 8. Let $\mathbb{E}_{R_s}[BCRB(R_s | x)]$ denote the average sensing cost. This quantity serves as an asymptotic lower bound for the function $c(x)$ defined in (8). Specifically, we have

$$BCRB(\mathbb{E}_{R_s}[R_s] | x) \leq \mathbb{E}_{R_s}[BCRB(R_s | x)] \leq c(x), \quad (17)$$

where the inequalities are asymptotic. This result supports DRT [5] in the asymptotic regime with a high number of sensing antennas.

Proof. The second inequality follows from [19, Theorem 3.1 and Theorem 11.3]. The first inequality follows from Jensen's inequality [16] and Lemma 7, with equality when $P_{R_s}(r_s)$ is deterministic. \square

Corollary 1. Based on lemma 8, the expected BCRB given R_s , $\mathbb{E}_{R_s}[BCRB(R_s | x)]$, serves as an OB for the optimal C-D region in asymptotic, unbiased scenarios. A more random R_s can enhance sensing performance by reducing variance, as distributions with higher randomness and more data records exhibit less variance around the mean (6), according to the central limit theorem (CLT). The distribution of the sample mean (optimal estimator in (6)) approaches normality as n_s increases, with variance decreasing by a factor of $\frac{1}{n_s}$ [4]. Conversely, a more deterministic R_s can increase variance, potentially degrading performance. In such cases, $P_{R_s}(r_s)$ heavily influences $P_{R_s|X, \mathbf{y}_s}(r_s | x, \mathbf{y}_s)$ in (15), limiting variance reduction even with more information (e.g., multiple antennas). High precision in $P_{R_s}(r_s)$ can also be problematic if it does not align with the true parameter value, leading to biased estimates, especially under incorrect or overly strong assumptions. However, if R_s is accurate, fewer n_s are needed to achieve similar performance, illustrating the trade-off in selecting $P_{R_s}(r_s)$. We term this the modified DRT⁵.

IV. NUMERICAL RESULTS

This section presents results based on Table I. For each estimator (MAP or MLE) and each $x \in \mathcal{X}$, we generate N_r samples of R_s from $P_{R_s} \sim \text{Exp}(\lambda)$ and N_y samples of the sensing signal \mathbf{Y}_s from $P_{\mathbf{Y}_s|x, r_s} \sim \mathcal{N}\left(\frac{RCSx}{r_s^4}, \sigma_s^2\right)$. The average sensing cost (MSE) is approximated by $c(x) \approx \frac{1}{N_r} \sum_{r_s^{[i]}} \frac{1}{N_y} \sum_{\mathbf{y}_s^{[j]}} (r_s^{[i]} - \hat{\xi}(x, \mathbf{y}_s^{[j]}))^2$. The expectation of the variance and bias are computed similarly.

In Fig. 2, as the O-SNR ($|x|$) increases and λ decreases from 0.5 (high value) to 0.3 (low value), MAP and MLE

⁵This trade-off is related to concepts such as the bias-variance tradeoff, prior-data balance, prior vs. likelihood strength, overfitting vs. underfitting, and regularization, as discussed in statistical inference and machine learning (ML) literature [4].

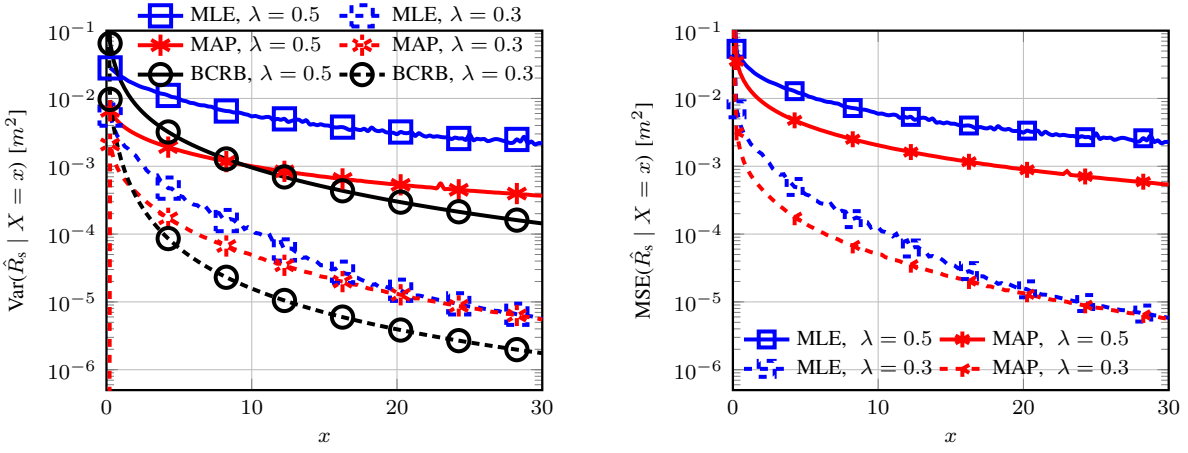


Fig. 2: Average performance metrics of multi-antenna sensing methods ($n_s = 64$).

TABLE I: Default Parameters

Parameter	Value
h_c (CC)	Deterministic, 1
η_0 (Initial Learning Rate)	1
γ (Decay Rate)	20
λ (Exponential Parameter)	0.3, 0.5 m^{-1}
RCS (Radar Cross-Section)	1 (perfect)
σ_s^2, σ_c^2 (Noise Variances)	1 W
P (Optical Power Budget)	10 W
q (Quantization Step)	0.25
Quantized Noise Range	$[-5 \times \sigma_s^2, 5 \times \sigma_s^2]$
Number of Sens. Rx Antennas	1 (single), 64 (multiple)
$x_{ \mathcal{X} }$ (Last Mass Point in \mathcal{X})	30

estimators approach together, confirming Lemma 5⁶. However, in the single-antenna case (figure omitted for brevity) with $n_s = 1$, the performance difference between $\lambda = 0.3$ and $\lambda = 0.5$ is more noticeable, as $P_{R_s}(r_s)$ has a greater impact with limited n_s . MLE and MAP are more biased, suggesting potential violations of regularity conditions, making BCRB an unreliable approximation of the estimator's performance (MSE). Additionally, Fig. 2 shows that in optimal C-D (not AR-CRB) region, DRT defined in [5] can be violated. A more random distribution ($\lambda = 0.3$) may yield better sensing performance, while a more deterministic one ($\lambda = 0.5$) may result in worse performance, as justified by Corollary 1 and the modified DRT.

Fig. 3a shows the optimized cumulative distribution function (CDF) for various modes in a multiple-antenna setting. The sensing-optimized input distribution, obtained via CVX [20], aligns with Lemma 2. We also present the high O-SNR CDF for the Comm. Opt. mode ($\text{Exp}(\frac{1}{E})$, from [14]) and a common point ($t = 10$) from the ISAC optimized region. The similarity of ISAC-optimized CDFs across approaches confirms Theorem 3 and lemma 5, showing that stricter distortion constraints shift probability mass to $X > \epsilon$ and concentrate probabilities at specific points, validating DRT of ISAC in FSO S-I Gaussian channels with multiple antennas [5].

Fig. 3b demonstrates that BCRB-based approaches behave

⁶Given $\sigma_c^2 = 1$, O-SNR simplifies to $|x|$.

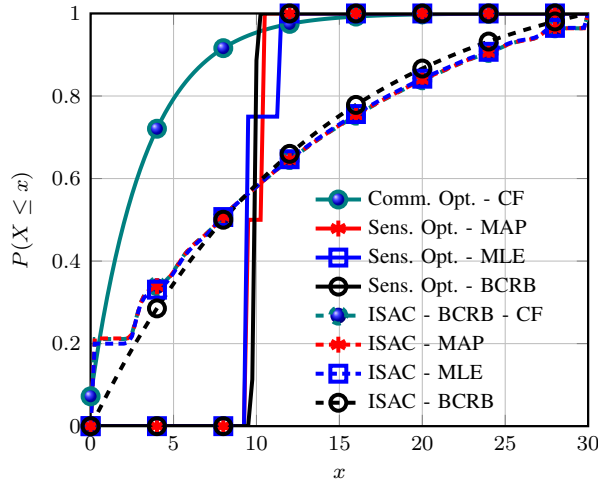
as an OB, with MAP and MLE covering larger regions due to lower MSE. Utilizing BCRB in multi-antenna settings narrows the gap between BCRB and MAP/MLE approaches. Sens. Opt. and Comm. Opt. modes validate BAA and CF algorithm across different estimators, showing MAP and MLE convergence as n_s increases. The results also indicate that the CF algorithm region closely aligns with BAA region.

CONCLUSION

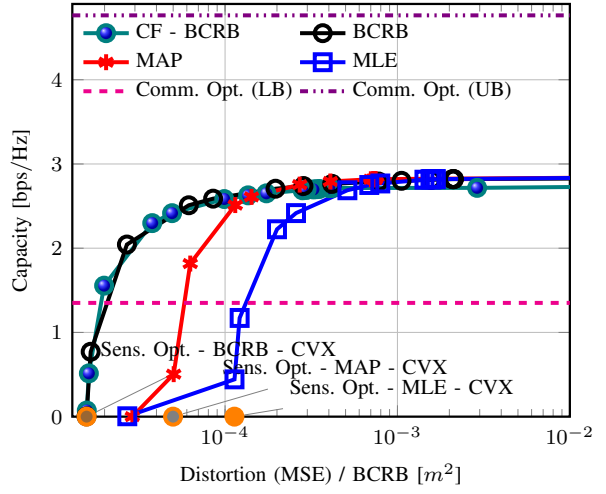
In this paper, we revisited the performance of O-ISAC from a C-D perspective. We developed practical MAP and MLE for target distance, showing their convergence to BCRB as the number of sensing antennas increases. Our analysis established AR-CRB as an asymptotic OB for the optimal C-D region. We also extended and modified DRT to this optical ISAC context, enhancing its applicability. Furthermore, we introduced iterative BAA-type and memory-efficient algorithms for deriving optimal input distributions. Notably, we proved that at high O-SNR, the optimal O-ISAC input distribution adopts an exponential-like form.

REFERENCES

- [1] F. Liu, L. Zheng, Y. Cui, C. Masouros, A. P. Petropulu, H. Griffiths, and Y. C. Eldar, "Seventy Years of Radar and Communications: The road from separation to integration," *IEEE Signal Process. Mag.*, vol. 40, no. 5, pp. 106–121, Jul. 2023.
- [2] Y. Wen, F. Yang, J. Song, and Z. Han, "Optical Integrated Sensing and Communication: Architectures, Potentials and Challenges," *IEEE Internet Things Mag.*, vol. 7, no. 4, pp. 68–74, Jul. 2024.
- [3] M. Ahmadipour, M. Kobayashi, M. Wigger, and G. Caire, "An Information-Theoretic Approach to Joint Sensing and Communication," *IEEE Trans. Inf. Theory*, vol. 70, no. 2, pp. 1124–1146, Feb. 2024.
- [4] S. J. Press, *Bayesian Statistics: Principles, Models, and Applications*. Wiley, May 1989.
- [5] Y. Xiong, F. Liu, K. Wan, W. Yuan, Y. Cui, and G. Caire, "From Torch to Projector: Fundamental Tradeoff of Integrated Sensing and Communications," *IEEE BITS Inf. Theory Mag.*, pp. 1–13, 2024.
- [6] H. Hua, T. X. Han, and J. Xu, "MIMO Integrated Sensing and Communication: CRB-Rate Tradeoff," *IEEE Trans. Wirel. Commun.*, vol. 23, no. 4, pp. 2839–2854, Apr. 2024.
- [7] Z. Ren, Y. Peng, X. Song, Y. Fang, L. Qiu, L. Liu, D. W. K. Ng, and J. Xu, "Fundamental CRB-Rate Tradeoff in Multi-Antenna ISAC Systems With Information Multicasting and Multi-Target Sensing," *IEEE Trans. Wirel. Commun.*, vol. 23, no. 4, pp. 3870–3885, Apr. 2024.



(a)



(b)

Fig. 3: (a) Optimized CDF for several modes, (b) C-D Region ($n_s = 64$).

- [8] M. Soltani, M. Mirmohseni, and R. Tafazolli, "Outage tradeoff analysis in a downlink integrated sensing and communication network," in 2023 IEEE Globecom Workshops (GC Wkshps), 2023, pp. 951–956.
- [9] T. Gomes, R. Roriz, L. Cunha, A. Ganal, N. Soares, T. Araújo, and J. Monteiro, "Evaluation and Testing System for Automotive LiDAR Sensors," *Appl. Sci.*, vol. 12, no. 24, p. 13003, Jan. 2022.
- [10] A. Elzanaty and M.-S. Alouini, "Adaptive Coded Modulation for IM/DD Free-Space Optical Backhauling: A Probabilistic Shaping Approach," *IEEE Trans. Commun.*, vol. 68, no. 10, pp. 6388–6402, Oct. 2020.
- [11] A. Kafizov, A. Elzanaty, and M.-S. Alouini, "Probabilistic constellation shaping for enhancing spectral efficiency in noma vlc systems," *IEEE Trans. Wirel. Commun.*, vol. 23, no. 8, pp. 9958–9971, 2024.
- [12] M. A. Richards, J. Scheer, W. A. Holm, and W. L. Melvin, *Principles of Modern Radar: Basic Principles*. IET Digital Library, Jan. 2010.
- [13] R. Fatemi, B. Abiri, A. Khachaturian, and A. Hajimiri, "High sensitivity active flat optics optical phased array receiver with a two-dimensional aperture," *Opt Express*, vol. 26, no. 23, pp. 29 983–29 999, Nov. 2018.
- [14] S. M. Moser, "Capacity Results of an Optical Intensity Channel With Input-Dependent Gaussian Noise," *IEEE Trans. Inf. Theory*, vol. 58, no. 1, pp. 207–223, Jan. 2012.
- [15] T. M. Cover and J. A. Thomas, *Elements of Information Theory (Wiley Series in Telecommunications and Signal Processing)*. USA: Wiley-Interscience, Jun. 2006.
- [16] S. Boyd and L. Vandenberghe, *Convex Optimization*. Cambridge University Press, Mar. 2004.
- [17] R. Blahut, "Computation of channel capacity and rate-distortion functions," *IEEE Trans. Inf. Theory*, vol. 18, no. 4, pp. 460–473, Jul. 1972.
- [18] A. W. van der Vaart, *Asymptotic Statistics*, ser. Cambridge Series in Statistical and Probabilistic Mathematics. Cambridge: Cambridge University Press, 1998.
- [19] S. M. Kay, *Fundamentals of Statistical Signal Processing: Estimation Theory*. USA: Prentice-Hall, Inc., Feb. 1993.
- [20] M. Grant and S. Boyd, "CVX: Matlab software for disciplined convex programming, version 2.1," <https://cvxr.com/cvx>, Mar. 2014.

APPENDIX A PROOF OF LEMMA 1

Proof. Following [3, Appendix A], where a scalar feedback observation on the i -th channel (denoted as z_i in [3], and $y_{s,i}$ here) is considered, we extend this to a vector of n_s independent observations. $\hat{\xi}^* = \int_{r_s \in \mathcal{R}_s} P_{R_s|X_s, \mathbf{y}_s}(r_s | x, \mathbf{y}_s) d(r_s, r'_s)$. Then, $c(x) = \mathbb{E}_{\mathbf{Y}_{s,i}|X_i} [\mathbb{E}_{R_{s,i}|X_i, \mathbf{Y}_{s,i}} [(R_{s,i} - \mu)^2]]$ \square

APPENDIX B NUMERICAL METHODS FOR SOLVING (9)

To derive the C-D region, we use GD for power allocation and BAA ($[P_i, D_i, \mathcal{I}_i, P_X^*] := \text{BAA} - F$) to optimize $s^{(i)}$ for each $t \in \mathcal{T}$, meeting the power budget and maximizing MI. In high O-SNR scenarios, CF algorithm in lemma 3 ($[P_i, D_i, P_X, \mathcal{I}_i] := \text{CFA} - F$) replaces $[P_i, D_i, \mathcal{I}_i, P_X^*] := \text{BAA} - F$.

Remark 3. In Algorithm 1, \mathcal{X} is quantized as: $\mathcal{X}_q = \{(m-1)q | m = 1, \dots, \frac{|\mathcal{X}|}{q} + 1\}$, where q is the quantization step. The Gaussian noise Z_c is quantized with step q^2 , denoted as Z_{c,q^2} . For small q , $\mathcal{X}_q \approx \mathcal{X}$ and $Z_{c,q^2} \approx Z_c$.

APPENDIX C PROOF OF LEMMA 2

Proof. Let us write the Lagrangian function for (12):

$$J = \int_{x \in \mathcal{X}} c(x) P_X(x) + \eta_4 \left(\int_{x \in \mathcal{X}} x P_X(x) - P \right) + \eta_5 \left(\int_{x \in \mathcal{X}} P_X(x) - 1 \right). \quad (18)$$

Differentiating J w.r.t. $P_X(x_i)$ for each i gives:

$$\frac{\partial J}{\partial P_X(x_i)} = c(x_i) + \eta_4 x_i + \eta_5.$$

Assuming $\eta_4 = 0$, we get $\eta_5 = -c(x_i)$ by complementary slackness, implying $c(x_i)$ must be constant, which is generally not the case. Hence, $\eta_4 \neq 0$. For the optimal solution, complementary slackness requires: $\int_{x \in \mathcal{X}} x_i P_X^{\text{Sens. Opt.}}(x_i) = P$. For a nonnegative random variable X , $\mathbb{E}[X] \geq \min(X)$, with equality if and only if X is almost surely constant and equal to $\min(X)$ [15, Theorem 2.6.1]. So, $\min c(x) \leq \int_{x \in \mathcal{X}} c(x) P_X(x)$. Thus, $P_X^{\text{Sens. Opt.}}(x) = \delta(x - x^*)$, where $x^* := \arg \min_{x \leq P} c(x)$. \square

Algorithm 1: BAA-type Algorithm for C-D Region

```

Input:  $\delta_{BA}$ ,  $\delta_B$ ,  $\mathcal{X}$ , and  $P$ 
Output:  $\{D^{(j)}\}_{j=1}^{|\mathcal{T}|}$  and  $\{\mathcal{I}^{(j)}\}_{j=1}^{|\mathcal{I}|}$ 
// BAA Function for general
1 Function  $[P_i, D_i, \mathcal{I}_i, P_X^*] := \text{BAA} - F(s^{(i)}, t, P_X)$ :
  Initialization:  $iter := 0$ 
  repeat
     $iter := iter + 1$ 
    if  $iter \neq 1$  then
       $P_X^* := \frac{P_X \odot g}{2^{\mathcal{I}_L}}$ 
     $g_k := \exp \left( \sum_{y_c \in Y_c} P_{Y_c|X}(y_c|x_k) \right.$ 
     $\times \log_2 \left( \frac{P_{Y_c|X}(y_c|x_k)}{\sum_{y_c \in Y_c} P_{Y_c|X}(y_c|x_k) P_X(x_k)} \right) \left. \right)$ 
     $\mathcal{I}_L := \log_2 \left( \sum_{x \in \mathcal{X}} g_k P_X(x_k) \right)$ 
     $\mathcal{I}_U := \log_2(\max_k g_k)$ 
     $iter := iter + 1$ 
  until  $|\mathcal{I}_U - \mathcal{I}_L| < \delta_{BA}$ 
  return
     $P_i = \mathcal{X}_q P_X, D_i = c(\mathcal{X}_q) P_X,$ 
     $\mathcal{I}_i = s^{(i)} \times P_i + t \times D_i + \mathcal{I}_L$ 
  // CF algorithm (CFA) for high O-SNR
12 Function  $[P_i, D_i, P_X, \mathcal{I}_i] := \text{CFA} - F(s^{(i)}, t)$ :
   $G_X(x) = \exp(-s^{(i)} \cdot x - t \cdot c(x))$ 
   $P_X := \frac{G_X(x)}{\sum_{j=0}^{|\mathcal{X}|} G_X(x_j)}$ 
   $P_i := \sum_{j=0}^{|\mathcal{X}|} x_j P_X(x_j)$ 
   $D_i := \sum_{j=0}^{|\mathcal{X}|} c(x_j) P_X(x_j)$ 
  return  $P_i, D_i, P_X$ , and  $\mathcal{I}_i$ 
// main
Initialization:  $P_X := \frac{1}{|\mathcal{X}|}, j := 1$ 
18 for  $t \in \mathcal{T}$  do
   $i := 0, s^{(0)} := 0$ 
   $[P_i, D_i, \mathcal{I}_i, P_X^*] := \text{BAA} - F(s^{(i)}, t, P_X)$ 
  /* or  $[P_i, D_i, P_X, \mathcal{I}_i] := \text{CFA} - F(s^{(i)}, t)$  */
  if  $P_i < P$  then
    Break
  else
     $i := 1, s^{(1)} := 1$ 
     $[P_i, D_i, \mathcal{I}_i, P_X^*] := \text{BAA} - F(s^{(i)}, t, P_X)$ 
    /* or  $[P_i, D_i, P_X, \mathcal{I}_i] := \text{CFA} - F(s^{(i)}, t)$  */
    repeat
       $\eta_k = \frac{\eta_0}{1 + \gamma \cdot (0,1)^k}, i := i + 1, ds := \frac{P_i - P_{i-1}}{s^{(i)} - s^{(i-1)}}$ 
       $s^{(i)} := \max\{0, s - \eta_k \frac{P_i - P}{ds}\}$ 
       $[P_i, D_i, \mathcal{I}_i, P_X^*] := \text{BAA} - F(s^{(i)}, t, P_X)$ 
      /* or  $[P_i, D_i, P_X, \mathcal{I}_i] := \text{CFA} - F(s^{(i)}, t)$  */
    until  $|P_i - P| < \delta_B$ 
   $D^{(j)} := D_i, \mathcal{I}^{(j)} := \mathcal{I}_i, j := j + 1$ 

```

The score function becomes:

$$\frac{\partial \log p_{Y_s|X, R_s}}{\partial r_s} = -\frac{1}{\sigma_s^2} \sum_{i=1}^{n_s} (y_{s,i} - \text{RCS}x r_s^{-4}) \cdot (4 \text{RCS}x r_s^{-3}) + \lambda. \quad (20)$$

The Fisher Information (FI) is:

$$I(r_s) = \frac{16n_s \text{RCS}^2 x^2 r_s^{-8}}{\sigma_s^2} + \lambda.$$

Thus, BCRB is:

$$\text{BCRB}(x | r_s) = \frac{1}{I(x, r_s)} = \frac{1}{\frac{16n_s \text{RCS}^2 x^2 r_s^{-8}}{\sigma_s^2} + \lambda}.$$

□

APPENDIX E PROOF OF LEMMA 7

Proof. To prove the convexity of $f(r_s) := \text{BCRB}(r_s | x)$, start by simplifying the function:

$$f(r_s) = \frac{1}{A r_s^{-8} + \lambda}, \quad \text{where } A = \frac{16n_s \text{RCS}^2 x^2}{\sigma_s^2}.$$

The first derivative is:

$$f'(r_s) = \frac{8A r_s^{-9}}{(A r_s^{-8} + \lambda)^2}.$$

The second derivative, using the quotient rule, is:

$$f''(r_s) = \frac{56A^2 r_s^{-8} - 72A\lambda}{(A r_s^{-8} + \lambda)^3}.$$

For convexity, $f''(r_s)$ should be non-negative. Since $A r_s^{-8}$ dominates for large A , $f''(r_s)$ is positive, proving the convexity of $f(r_s)$. □

APPENDIX D

PROOF OF THEOREM 3

Proof. For n_s samples, the log-likelihood function is:

$$\log p_{Y_s|X, R_s} = -\frac{n_s}{2} \log(2\pi N) - \frac{1}{2\sigma_s^2} \sum_{i=1}^{n_s} (y_{s,i} - \text{RCS}x r_s^{-4})^2. \quad (19)$$